Hydrol. Earth Syst. Sci. Discuss., 12, 9655–9700, 2015
www.hydrol-earth-syst-sci-discuss.net/12/9655/2015/
doi:10.5194/hessd-12-9655-2015

Hydrology and Earth System Sciences
Open Access
Discussions

Co-evolution of volcanic catchments in Japan

T. Yoshida[1,2] **and P. A. Troch**[1]

[1]University of Arizona, Tucson, AZ, USA
[2]National Agricultural Research Organization, Tsukuba, Ibaraki, Japan

Received: 26 August 2015 – Accepted: 29 August 2015 – Published: 24 September 2015

Correspondence to: T. Yoshida (takeoys@affrc.go.jp)

Published by Copernicus Publications on behalf of the European Geosciences Union.

Abstract

Present day landscapes have evolved over time through interactions between the prevailing climates and geological settings. Understanding the linkage between spatial patterns of landforms, soils, and vegetation in landscapes and their hydrological response is critical to make quantitative predictions in ungaged basins. Catchment co-evolution is a theoretical framework that seeks to formulate hypotheses about the mechanisms and conditions that determine the historical development of catchments and how such evolution affects their hydrological response. In this study, we selected 14 volcanic catchments of different ages (from 0.225 to 82.2 Ma) in Japan. We derived indices of landscape properties (drainage density) as well as hydrological response (annual water balance, baseflow index, and flow duration curves) and examined their relation with catchment age and climate (through the aridity index). We found significant correlation between drainage density and baseflow index with age, but not with climate. The age of the catchments was also significantly related to intra-annual flow variability. Younger catchments tend to have lower peak flows and higher low flows, while older catchments exhibit more flashy runoff. The decrease of baseflow with catchment age confirms previous studies that hypothesized that in volcanic landscapes the major flow pathways have changed over time, from deep groundwater flow to shallow subsurface flow. The drainage density of our catchments decreased with age, contrary to previous findings in similar volcanic catchments but of significant younger age than the ones explored here. In these younger catchments, an increase in drainage density with age was observed, and it was hypothesized that this was because of more landscape incision due to increasing near-surface lateral flow paths in more mature catchments. Our results suggests two hypotheses on the evolution of drainage density in matured catchments. One is that as catchments further evolve, hydrologically active channels retreat as less recharge leads to lower average aquifer levels and less baseflow; the other is that it does not significantly change after catchments reached maturity in terms of surface dissection.

HESSD

12, 9655–9700, 2015

1 Introduction

The hydrological functions that partition incoming water, energy and carbon at the land surface vary from place to place, reflecting spatial variability in land surface characteristics (landforms, soils, vegetation). Because of this spatial variability, hydrological predictions in ungaged basins are highly uncertain (Wagener et al., 2007; Sivapalan, 2003). Improving these predictions will require a better understanding of the different interactions between landscape features and hydrological response, especially in a changing environment (McDonnell et al., 2007; Wagener et al., 2013).

Present day land surface characteristics in pristine landscapes have co-evolved over time through various interactions between the prevailing climates and geological settings (bedrock type, tectonic uplift) (Blöschl et al., 2013; Troch et al., 2015). Hydrologists have coined the term catchment co-evolution as a theoretical framework that seeks to formulate explanatory hypotheses about spatial patterns of landscape characteristics and the corresponding hydrological response, based on the historical development of catchments (Sivapalan et al., 2012; Troch et al., 2013; Harman and Troch, 2013). The results of historical development are captured in the soil and hillslope catena profiles, the geometry of channel networks and the spatial distribution of plant functional types. This landscape organization determines the hydrological functions that partition incoming water, energy and carbon. A detailed mechanistic reconstruction of how catchments have evolved to its present state is a daunting task, given the many processes involved and the unknown initial conditions during landscape formation.

Therefore, formulating and testing explanatory hypotheses of catchment co-evolution and hydrological response requires a different approach from the classic mechanistic Newtonian approach. Recently, an alternative approach, called Darwinian hydrology, was proposed that seeks to document patterns of variation in populations of hydrological systems, and explain these patterns in terms of the processes and conditions of their historical development (Wagener et al., 2013; Harman and Troch, 2013). Har-

HESSD
12, 9655–9700, 2015

man and Troch (2013) summarized what the Darwinian approach might look like in watershed science as follows:

1. collect extensive and detailed observations of the pattern to be explained,
2. conceive a hypothesis that accounts for as many of the observations as possible,
3. derive from this hypothesis a subsequent set of circumstances that also must hold if the hypothesis is true, and
4. critically test whether these consequences do hold.

In this study, we build upon this framework and explore empirically the links between landscape properties, hydrological response, and time since formation (age) of catchments of similar bedrock geology (volcanic rock deposits of different geologic age).

It might be argued that climate exerts a first-order control on hydrologic partitioning and that physical, chemical and biological catchment properties only have a second-order impact (e.g., Berghuijs et al., 2014; Sivapalan et al., 2011). However, these second-order controls explain much of the functional patterns that determine flow regimes. Mushiake et al. (1981) observed that bedrock lithology plays a key role in the natural variations of functional patterns in Japanese catchments. They showed that catchments on older sedimentary rocks formed in the Paleozoic and Mesozoic exhibit flashy hydrographs and low baseflow component compared to younger catchments on volcanic rock. They also found that catchments underlain by younger volcanic rock formed in the Quaternary have a greater groundwater component compared to those on older volcanic rock formed in the Tertiary. Lohse and Dietrich (2005) found that vertical saturated hydraulic conductivity declines as volcanic soils in Hawaii develop with time, due to the formation of secondary clay mineral layers in those soil profiles. This evolution impedes rates of vertical percolation of water and encourages increase of shallow lateral subsurface flow. Jefferson et al. (2010) studied landscape and hydrological signatures in basalt catchments in the Oregon Cascades and reported that

HESSD
12, 9655–9700, 2015

springs were absent in older catchments, which exhibit well-developed drainage networks and flashy hydrographs. They hypothesized that the differences in hydrological response between young and old catchments was the result of changes in flow pathways, from vertical recharge and groundwater dominated flow to shallow subsurface lateral flow with sufficient erosive power to create channel networks through landscape incision.

Prior work has suggested that climate controls variations in hydrologic regimes in two ways. One is the direct control on the water balance in function of available water and energy (e.g., Budyko, 1974; Milly, 1994; Troch et al., 2009; Sivapalan et al., 2011). The other is the indirect control on hydrologic regime as one of four independent factors (climate, bedrock weatherability, tectonic uplift and time) that control the evolution of landscape properties (landform, soil, and vegetation, Troch et al., 2015). For example, Gentine et al. (2012) found that catchment-scale rooting depth was strongly correlated with the seasonal distribution of water and energy availability in 431 catchments in the US. Wang and Wu (2013) found strong inverse correlation between perennial stream density and climate aridity index in 185 catchments across the US. Both studies suggest that these catchments evolved by adapting to the long-term climate conditions.

From this overview it is clear that both climate and time influence spatial variations of hydrological response. In this study we investigate the level of control of climate and time on the differences in hydrological response between catchments that have different internal organizations. More specifically, we ask the following questions: (1) how do landscape features and hydrological response differ with catchment age and climate? (2) What is the dominant control of catchment co-evolution in basaltic landscapes? (3) What are the possible mechanisms related to the historical development of volcanic catchments? To address these questions we selected 14 catchments dominated by basaltic rock with different ages and from a range of climatic regions of Japan. The age of the catchments ranges from 0.225 to 82.2 Ma (million years). The aridity index (ratio of annual potential evaporation to annual precipitation) for these catchments ranges from 0.28 to 0.82. For each catchment we derived indices of landscape features

HESSD
12, 9655–9700, 2015

(drainage density) and hydrological response (annual water balance, baseflow index, and flow duration curves). We then used regression to explore possible relationships between these features and catchment age and climate, respectively.

2 Study area and materials

2.1 Study catchments

The study area is located within the Japanese archipelago, where 28 % of the land is underlain by volcanic rock. The makeup of the volcanic landscape in Japan with respect to time since formation, or geological age, is as follows: 11 % was formed in the Quaternary, 12 % in the Neogene, 1 % in the Paleogene, and 4 % in the Cretaceous (Murata and Kano, 1995). The volcanic landscapes formed in the Quartenary and Neogene are mostly prevalent in north-eastern and south-western Japan, and those formed in the Paleogene and Cretaceous are predominantly in central and western Japan. The majority of the basement rock of Japan was formed in the Jurassic to Paleogene at the margin of the Asian Continent and moved toward the current position during the spreading of the Japan Sea Basin in the Neogene (Taira, 2001). The volcanic rocks formed in the Cretaceous, which are prevalent in western Japan, was formed at the marginal area of the Asian Continent and exposed to the atmosphere since their formation. The volcanic rocks of the Quaternary and Neogene age, on the other hand, were formed after the spreading of the Japan Sea Basin and thus have lain in their current position since their formation.

The catchments selected for the study are among the catchments listed in the Japanese Dam Database (National Institute for Land and Infrastructure Management, Japan, 2015). Out of 130 catchments listed in the database, we selected 14 that contain more than 50 % volcanic rock coverage (Table 1). Basalt is the dominant rock type in all cacthments, while rhyolite is found in five of the catchments (GOS, YUD, AIM, IKR, and KWM), but at less than 15 % of the volcanic rock area. The catchment area

HESSD
12, 9655–9700, 2015

ranges from 30.9 to 635.0 km^2. Daily streamflow observed at each dam was obtained from the Japanese Dam Database. The streamflow observations are inflow to the dams and no major dams are located upstream, therefore those streamflows are not affected by human regulations.

The catchment ages were assigned from the average of the ages of different volcanic rocks, weighted by area of coverage, obtained from the Seamless Geological Map of Japan (Geological Survey of Japan, 2012). The map is the product of the merged 1 : 200 000 geologic map sheets covering the entire country of Japan. The age of the catchments ranges from 0.225 to 82.2 Ma. The youngest catchment (SNK) is located in central Japan (Fig. 1). The oldest catchment (HAZ) is covered with basalt formed in Late Cretaceous (Fig. 2). The other 12 catchments were formed in the Neogene period (2.7–18.5 Ma) and are clustered in north-eastern Japan, with the exception of the Shimouke catchment in southern Japan.

To delineate catchments, digital elevation models (DEMs) of 10 m × 10 m were downloaded from the website of Geographic Survey Institute, Japan (2015). The stream networks were derived from digitized GIS maps from the National Land Numerical Information website (Ministry of Land, Infrastructure and Transportation, Japan, 2015).

2.2 Meteorological data

A 20 year (from 1993 through 2012) meteorological dataset (including precipitation, temperature, humidity, and wind speed) was distilled from a gridded dataset (hereafter referred to as the raw dataset). The gridded dataset covers all of Japan with grid cells of approximately 1 km × 1 km in size. The data interpolation was performed using observed data from the Automated Meteorological Data Acquisition System (AMeDaS) of Japan and the Mesh Climate Data 2000 (Japan Meteorological Agency, 2002). The Mesh Climate Data 2000 provides estimated of monthly climatic means from 1971 through 2000 for these grid cells by empirical relationships to account for orographic effects. The details of the raw dataset are described in the Appendix.

HESSD
12, 9655–9700, 2015

3 Methods

3.1 Correction of meteorological data

The precipitation in the raw dataset accounts for orographic effects based on empirical relationships between precipitation and geographic features, such as elevation and distance from shoreline. It may hence not represent local orographic effects (e.g., higher rate of increase in precipitation on windward side of mountains), nor does it correct for snow undercatch. Thus, we corrected the precipitation data as described in the Appendix. We assessed the validity of the raw and corrected datasets by means of the long-term water balance of the catchments. Given the mean of catchment-normalized annual precipitation for the raw dataset P_{raw} ($mm\,yr^{-1}$) and precipitation-corrected dataset P_{cor} ($mm\,yr^{-1}$), and streamflow, Q ($mm\,yr^{-1}$), we estimated the mean annual evapotranspiration for each of the dataset, E_{raw} and E_{cor} ($mm\,yr^{-1}$), as follows:

$$E_{raw} = P_{raw} - Q \quad (1)$$

$$E_{cor} = P_{cor} - Q. \quad (2)$$

To cross-check the acceptability of E_{raw} and E_{cor}, catchment-scale actual evapotranspiration, E_a ($mm\,yr^{-1}$), was directly estimated with the complementary relation method (e.g., Bouchet, 1963; Morton, 1978; Brutsaert and Stricker, 1979). In this study, the complementary relationship method proposed by Otsuki et al. (1984) was used to estimate E_a for each catchment. The method was used because it was rigorously validated with the long-term evapotranspiration in several experimental watersheds across Japan and does not require additional parameters.

Thus we have three types of meteorological datasets to estimate the long-term water balance:

- raw dataset: P_{raw}, E_{raw},
- corrected P dataset: P_{cor}, E_{cor},

HESSD
12, 9655–9700, 2015

– estimated E dataset: P_{cor}, E_a.

The estimated data were validated aganist the Budyko hypothesis (Budyko, 1974). Budyko (1974) postulated an empirical relationship between the long-term evaporation index, E/P, and the aridity index, PE/P, and argued that this relationship can be satisfactorily applied to most catchments. The large bias or discrepancy of estimated evaporation from the prediction of the Budyko curve was interpreted to derive from errors in the dataset (Fig. 3).

3.2 Geomorphologic and hydrological signatures

Drainage density is defined as the total length of streams divided by catchment area ($km\,km^{-2}$). To obtain the stream length, we used the length of the vectors defining blue-colored streamlines in the digitized version of topographic maps (Geographic Survey Institute, Japan, 2015). Because our study catchments are all located in humid regions where precipitation is evenly distributed, we assumed that the blue lines of our digital dataset represents perennial streams.

Two signatures were used to represent the hydrological response of the study catchments. The first one is the baseflow index, the ratio of long-term baseflow component to total streamflow (e.g., Vogel and Kroll, 1992; Kroll et al., 2004). The higher the baseflow index the higher the groundwater contribution to catchment outflow. We separated the baseflow component from total streamflow as follows:

$$Q_b(t) = \epsilon Q_b(t-1) + \frac{1-\epsilon}{2}\left(Q(t) - Q(t-1)\right), \quad (3)$$

where $Q_b(t) = Q(t)$ when $Q_b(t) > Q(t)$; $Q(t)$ is total streamflow at time t, $Q_b(t)$ is the estimated baseflow, and ϵ is a low-pass filter parameter (Arnold and Allen, 1999; Eckhardt, 2005). To compare hydrological responses among catchments consistently, the filter parameter ϵ was set at 0.925 for all catchments (Sawicz et al., 2011).

To quantify an index of flow variability, the slope of the flow duration curve was used as the second signature. The flow duration curve is the cumulative probability distri-

HESSD
12, 9655–9700, 2015

bution of daily streamflow. The slope of the flow duration curve is calculated between the 33rd and 66th streamflow percentiles, because this range represents a relatively linear part of the flow duration curve on semi-log scale (Yadav et al., 2007; Zhang et al., 2008). This is caluculated from

$$S_{\mathrm{fdc}} = \frac{Q_{33} - Q_{66}}{0.66 - 0.33}, \tag{4}$$

where Q_{66} and Q_{33} are the streamflows that correspond to 66 and 33 % exceedance probability, respectively. A high slope value indicates a variable flow regime, while a low slope value means a more damped response. A damped response can arise as a result of a combination of persistent (wide-spread and year-round) precipitation, dominance of groundwater contribution to streamflow, or a combination of the two.

4 Results

4.1 Initial data evaluation

To evaluate data consistency with long-term water partitioning, we plot evaporation index versus aridity index for all catchments and compared them against the Budyko curve (Fig. 3). The plotted data points for the raw dataset are all well below the Budyko curve. Catchment-scale actual evapotranspiration, E_{a}, estimated from the complementary relation method, on the other hand, showed good agreement with the Budyko curve, suggesting realistic representation of long-term evapotranspiration in each of the catchment.

Errors in the estimates of the raw dataset could be caused by errors in discharge observations, trans-boundary groundwater flux, and catchment-averaged precipitation. The discharge, or dam inflow, was validated with the dam outflow, and the bias in the total inflow to total outflow was less than 2 % over 20 years. We thus assume that the dam inflow data is reliable. Another potential error is trans-boundary groundwater flux.

HESSD
12, 9655–9700, 2015

Quantifying this flux is very difficult; however, by focusing on relatively large catchments ($> 30\,km^2$), we argue that the influence of such a flux is negligible. It is more likely that the errors in annual evaporation estimated from the water balance are caused by underestimation of areal precipitation from the gridded data. Indeed, the corrected precipitation dataset showed substantial improvement from the raw dataset compared to the Budyko's hypothesis although some data still plot below the Budyko curve, likely caused by additional precipitation underestimation due to snow undercatch.

The aridity indices calculated with P_{cor} were hence used for subsequent analysis (Table 2). All the catchments lie in a energy limited region (i.e., $PE/P < 1$). A weak correlation between climate aridity indices and catchment ages was found ($R = 0.501, p = 0.068$); thus, it is not possible to thoroughly investigate the controls of climate and time on catchment co-evolution because the oldest catchment lies in the driest region, while the youngest catchment lies in a humid region (Fig. 4).

4.2 Analysis by geological age: controls of time on catchment co-evolution

All the landscape and hydrological indices obtained from the analysis are presented in Table 3. Among them, baseflow index, drainage density and slope of flow duration curve were all strongly correlated with catchment age (Figs. 5 and 6). Figure 5 shows strong correlation between baseflow index and catchment age ($R = -0.756$, $p = 0.0017$), and drainage density and catchment age ($R = -0.603$, $p = 0.0222$), respectively. Because the catchment age spans three orders of magnitude, log (catchment age) was used in the analysis. The oldest catchment (HAZ) has a baseflow index of 0.533, while in the youngest catchment (SNK), the baseflow index of 0.835, highest among the study catchments, suggesting groundwater dominant flow regime. No significant correlation was found between the hydrologic indices between catchment age; the baseflow index ($R = -0.24$, $p = 0.42$) and drainage density ($R = 0.23$, $p = 0.43$).

The decrease in baseflow index with age was supported by the slope of the flow duration curves (Fig. 6). The slopes of the flow duration curve were positively correlated

HESSD
12, 9655–9700, 2015

with catchment age (R = 0.74, p = 0.002), i.e., as catchments age, the slope of the flow duration curve increases, indicating flashier runoff.

The flow duration curves for all the study catchments are presented in the inset of Fig. 7, in which each line represents the data from a certain range in aridity index. It is clear that the aridity index controls the total amount of generated streamflow, i.e., the higher the aridity index, less streamflow is generated by the catchment. Figure 7 depicts the flow duration curves for the catchments whose aridity index are in the range between 0.35 and 0.45. The slopes of the flow duration curves of relatively young catchments, less than 4 Ma, were noticeably less than the older catchments. This implies that flowpaths in older catchments with similar aridity index have changed from deep groundwater to surface or near-surface flowpaths.

4.3 Analysis by climate: climate controls on catchment co-evolution

The drainage density and baseflow index shows no significant correlation with aridity index (Fig. 8), although there are decreasing trends in both.

Wang and Wu (2013) showed a systematic decrease in perennial stream density with increasing aridity index in 185 catchments in the US, with aridity indices ranging from 0.26 to 5.50 (Fig. 9). We assume that the digital stream dataset represents perennial streams because our study catchments are all located within humid regions, hence the drainage density is able to be compared with the perrenial stream density of Wang and Wu (2013). However, the curve of perennial stream density as a function of the aridity index derived by Wang and Wu (2013) does not explain the decreasing trend in drainage density of our catchments (inset of Fig. 9) even though the plotted data of our catchment cluster around the MOPEX catchment data (Fig. 9). In addition, no correlation was found between baseflow index and aridity index, not even in the US (Fig. 10). These results indicate that the partitioning of total runoff into baseflow and quick flow was not dominantly controlled by climate, at least in the narrow range of aridity index of our catchments, leaving the catchment age to be the strongest candidate as a predictor of the variability in baseflow index.

HESSD
12, 9655–9700, 2015

5 Discussion

This study was predicated on the assumption that there is a connection between geological age, climatic conditions and hydrological response. The data in our study support the hypothesis that catchment geologic age is the dominant descriptor for explaining variability in hydrologic response among volcanic catchments. Our results show that there are significant negative correlations between geologic age, baseflow index and drainage density. Variability in the baseflow index and flow duration curves suggest that younger catchments tend to have a larger groundwater flow component, while older catchments exhibit more flashy runoff. The decrease in baseflow in older catchments suggests that the major flow pathways have changed over time from deep groundwater aquifers to shallow subsurface flows.

The observed decrease of baseflow index with catchment age is consistent with the one observed in the Oregon Cascades in the western US (Fig. 11, Jefferson et al., 2010). The dataset that integrates those of Jefferson et al. (2010) and ours showed steeper decline of the baseflow index with catchment age and more significant correlation between them ($R = -0.879$, $p < 0.001$) than those for the catchments in Japan alone. They concluded that this decrease is the result of decreasing groundwater recharge due to a development of clay layers in the near subsurface (Lohse and Dietrich, 2005). The emergent negative trend of baseflow index for the integrated datasets suggests that the clay layers have continued to develop over longer periods than suggested by Jefferson et al. (2010).

The consistency in the decline rate of baseflow index with time since formation suggests the similarity in catchment evolution rate in both studies. Troch et al. (2015) proposed the concept of hydrological age in catchment co-evolution; i.e., "the age of a catchment is not only a function of time since formation, but also a function of how "active" the climate, geology, and tectonics are to drive coevolution". The aridity indices and annual precipitation for the catchments in Oregon Cascades are in the range from 0.5 to 1.0 (Zomer et al., 2008), and from 1800 to 2700 mm (Jefferson et al., 2010),

HESSD
12, 9655–9700, 2015

respectively. These conditions are in the same range of our study (aridity index: 0.281–0.826; annual precipitation: 1513–3305 mm) that allow the two studies to be compared.

A strong negative correlation was also found between the drainage density and catchment age. This finding contradicts prior work of Jefferson et al. (2010). The disparity may arise from the differences in catchment age. The age of our study catchments ranges from 0.225 to 82.2 Ma, while the ages of the catchments in the Oregon Cascades range from 0.017 to 15.5 Ma (Jefferson et al., 2010). From the global dataset of visible dissection on volcanic islands, Jefferson et al. (2014) observed that the visible dissection begins after about 0.5 Ma, that the dissection rate is much faster in humid landscapes, and that there is a transition from weak dissection to substantial dissection between 0.5 to 2 Ma, even in arid environment. Conversely, Suzuki (1969) observed the dissection in volcanic landscape in Japan and noted the dissection rates declined remarkably after 0.1 Ma after initiation of the dissection process. These data suggest that the increase in drainage density in the Oregon Cascade arose as a result of more intense surface dissection, whereas the catchments of our study possibly reached maturity in terms of dissection. Therefore, we hypothesize that the decline in drainage density with catchment age is caused by an additional mechanism than the one described in Jefferson et al. (2010).

In early stages of volcanic catchments development, most of the infiltrated water flows vertically due to the high permeability of the young basalt, which typically contains many cracks and fissures (Lohse and Dietrich, 2005). As time progresses, subsurface impermeable layers develop due to chemical weathering and mineral precipitation, and the major flow pathways change to shallow subsurface flow, rather than vertical flow. This change would result in a shorter transit time of water and flashy hydrological responses. As chemical weathering further continues, recharge to deep aquifers decreases, and further disconnection of the channel network from aquifers would result in a decrease in drainage density. This mechanism of decrease in drainage density with less groundwater recharge is supported by the data from Wang and Wu (2013). Figure 12 shows the relation between perennial stream density and baseflow coef-

HESSD
12, 9655–9700, 2015

ficient, Q_b/P for the MOPEX sites. The general trend is that catchments with lower baseflow coefficients tend to have lower drainage densities. The decline of drainage density with age therefore suggests that the portion of precipitation that recharges groundwater aquifers reduces with age.

However, plotting drainage density of our study with those observed in the western US gives us a different interpretation of the data (Fig. 13). First, the youngest catchment in our dataset, SNK, has much higher drainage density (1.08 km km^{-2}) than those of the similar age in the Oregon Cascades. Second, if we remove SNK, no significant correlation between the drainage density and catchment age can be found for the study catchments, although they still exhibits negative trend ($R = -0.32$, $p = 0.28$). From the lines (b) and (c) in Fig. 13, we can formulate an alternative hypothesis, that is, the volcanic catchments reach maturity in terms of the surface dissection approximately 2 Ma since their formation, and the drainage density does not change significantly after that.

To test these hypotheses, we investigated why the SNK catchment has such a high drainage density. The Digital Elevation Model of SNK reveals the distinct landscape differences in the upstream and downstream; i.e., less dissected plateau in the upstream and highly dissected valleys in the downstream (Fig. 14). The longitudinal profile of the longest stream in SNK shows a point of convexity, or a knick point, defined as a steep reach between two low gradient reaches (Fig. 15). The knick point is interpreted as a hallmark of transient state of a river system caused by changes in the lithology across which river flows, changes in tectonic uplift rate, or spatial variability in climate forces (Anderson and Anderson, 2010). The detailed investigation of the causality of the knick point is beyond the scope of this paper; however, it is noteworthy that the basalt in the upstream is younger than that in the downstream.

By dividing the catchment with the contour line of 1700 m where the stream gradient is the steepest (Fig. 15), we obtain the weighted average of the basalt age for the upper and lower areas as 72 and 380 kyr, and the drainage densities for those areas as 0.51 and 1.35 km km^{-2}, respectively. The plotted drainage density for the upper

HESSD
12, 9655–9700, 2015

part of SNK is comparable with those observed in the Oregon Cascades; however, the high drainage density for the lower part of the catchment cannot be explained (squares connected with the plot of SNK in Fig. 13). One possible explanation for the high drainage density in the lower part of the catchment is the acidity of stream water. The pH of the streamflow is as low as 2–3 due to high content of sulphuric acid (Ossaka et al., 1980). Especially, the lower part of the catchment is known for numerous hot springs that may dissects the landscape in much faster rate than neutral water. If it is the case that the extremely high drainage density in the lower part of SNK is caused by weathering due to acid streamflow, it can be an evidence that support the latter hypothesis, although this cannot reject the former one.

6 Conclusions

In this study, we selected 14 volcanic catchments that have different ages, ranging from 0.225 to 82.2 Ma. In these catchments, we derived indices including landscape features (e.g., drainage density) and hydrological responses (e.g., baseflow index, annual water balance and slope of flow duration curve). As a result, we revealed that the age of volcanic rock have significant connection to intra-annual or seasonal water balance. Younger catchments tend to have larger component of groundwater flow, while older ones exhibit more flashy hydrographs. The decrease in baseflow suggests that the major flow pathways have changed from deep groundwater aquifers to shallow subsurface flows. We also revealed that the drainage densities of the catchments have decreased with catchment aging. Although drainage density is controlled by the aridity index to some extent, catchment age has a more significant impact on the changes in drainage density. Our results suggests two hypotheses to be tested in future studies on the evolution of drainage density in matured catchments. One is that as catchments further evolve, hydrologically active channels retreat as less recharge leads to lower average aquifer levels and less baseflow; the other is that it does not significantly change after catchments reached maturity in terms of surface dissection. The fact that there is

HESSD
12, 9655–9700, 2015

a large number of potentially significant correlations between several landscape factors and hydrological responses allow us to enhance the predictive capabilities in different environments (e.g., Sivapalan et al., 2011; Troch et al., 2013; Harman and Troch, 2013).

The interconnected nature of landscape evolution and hydrologic co-evolution make it difficult to determine causality. Separating the effects of climate and base rock geology is difficult if we are restricted to empirical analysis. In addition, the weak correlation between climate gradient and catchment ages in our study catchments is also a confounding influence. One way to test the hypothesis in such an environment is to use process-based hydrological models in an attempt to derive responses that are not observable with direct measurement. For instance, Troch et al. (2013) decoupled the landscape and climate properties using a hydrological model developed by Carrillo et al. (2011) and illustrated how catchment characteristics varied with climate gradients.

Appendix A: Raw meteorological data

Required meteorological data (precipitation, temperature, relative humidity, and wind speed) were collected from 1976 through 2008 at existing observation stations. The meteorological data were obtained from the database of the Automated Meteorological Data Acquisition System (Japan Meteorological Agency). To estimate the spatial variation in the observed meteorological variables, the inverse distance weighting method was employed. In this method, the grid cell values are determined by calculating the weighted average of values observed at observation stations in the neighborhood of each grid cell. The closer a station is to the center of the cell being estimated, the greater its weight in the averaging.

Precipitation $p(x)$ (mm day^{-1}) in grid cell x was estimated by calculating the average of data from three observation stations, weighted according to the distance from x to the observation station. Then, the ratio of the observed precipitation to the estimated climatic value $r(i)$ (where $i = 1, 2, 3$) in the grid cell of station i was calculated as follows:

HESSD
12, 9655–9700, 2015

$$r(i) = p_o(i)/p_m(i), \quad \text{(A1)}$$

where $p_o(i)$ (mm day^{-1}) is the observed precipitation at station i and $p_m(i)$ (mm day^{-1}) is the climatic value derived from Mesh Climatic Data 2000, which is the monthly climatic precipitation for the corresponding Basic Grid Square (Third Area Partition) estimated from the observed spatial distribution of rainfall from 1971 through 2000 (Japan Meteorological Agency, 2002).

Then, ratio $r(i)$ is interpolated to each grid square of the model by using the inverse distance weighting method as follows:

$$r(x) = \sum_{i=1}^{3} \frac{w(i)r(i)}{\sum_{j=1}^{3} w(j)} \quad \text{(A2)}$$

$$w(i) = \frac{1}{d(x,i)^2}, \quad \text{(A3)}$$

where $d(i)$ is the distance from grid cell x to observation station i.

Finally, $p(x)$ is estimated by multiplying $r(i)$ by $p_m(i)$. Ideally, the estimated grid cell x should be located within a triangle formed by the three observation points; however, the same procedure was applied for grid cells outside of such a triangle. The values of other meteorological variables used for ET estimation were similarly interpolated by using the inverse distance method.

A1 Correction of meteorological data

A1.1 Precipitation corrected dataset

Precipitation was corrected by accounting for local orographic effects and undercatch of snow due to wind. To account for the orographic effect in complex terrain, we collected the observed precipitation in mountainous areas from the database of Water

HESSD
12, 9655–9700, 2015

Information System in Japan (online address: http://www1.river.go.jp/). These observation data provides more reliable local orographic effects and potentially improves the estimated precipitation in the raw dataset, P_{raw}. However, they are not consistent in the record length and often lacks data in winter due to heavy snow. Thus, we first sampled the precaipitation data, P_{obs}, observed in each study catchment whose record length is at least five years. We then aggregated P_{raw} and P_{obs} into annual averaged values and plotted them with the elevation of the grid cells and observed stations, respectively. In snow dominant areas where precipitation data is not available in winter, we aggregated the data only in summer during which the data is available. In those cases, we define P_{obs} as the mean precipiation for the sampling periods.

The comparison of the regressed lines showed the degree of underestimation for precipitation in each catchment. Figure A1 illustrates P_{raw} and P_{obs} in the HAZ catchment, where no data was missing in winter. We corrected P_{raw} so that the regressed line of P_{raw} agrees to that of P_{obs}. The results of this correction is defined as orographic-corrected dataset, P_{orog}.

Figure A2 compares P_{raw} and P_{obs} that were calculated from May through October, when the observation data is available in the ASE catchment, a typical snow dominant catchment. We corrected P_{raw} for the entire period by using the relationship obtained in Fig. A2. This might be a reason for the underestimation of P_{cor} shown in Table 2.

Next, the snow undercatch is corrected as follows. The daily precipitation P_{orog} was classified into snowfall P_{snow} and rainfall P_{rain} depending on the daily average temperature T_a. The value of $T_a = 2.2\,^{\circ}\mathrm{C}$ was used for the classification. The correction of snow undercatch was only applied with P_{snow} with undercatch ratio C_r:

$$C_r = \frac{1}{1 + mU}, \tag{A4}$$

where m is a specific parameter that depends on the type of raingauge (Yokoyama et al., 2003) and U is daily averaged wind speed ($\mathrm{m\,s^{-1}}$). The typical value of m was set to 0.346 for for the AMeDAS raingauges.

HESSD
12, 9655–9700, 2015

The precipitation dataset corrected with the above-mentioned procedures was defined as Precipitation-corrected dataset P_{cor}, calculated as follows:

$$P_{cor} = P_{snow}/C_r + P_{rain}. \quad \text{(A5)}$$

The mean annual evaporation calculated from the water balance with corrected precipitation P_{cor} was estimated as E_{cor}.

$$E_{cor} = P_{cor} - Q \quad \text{(A6)}$$

A2 Evaluation with catchment water balance

We evaluated the monthly water balance for each of dataset with a simple water balance model.

$$S(m) = S(m-1) + P(m) - \mathrm{AET}(m) - Q(m), \quad \text{(A7)}$$

where $S(m)$ is catchment storage in month m (mm), $P(m)$ is monthly precipitatin (mm), AET(m) is monthly actual evapotranspiration (mm), $Q(m)$ is monthly observed streamflow normalized by catchment area (mm). AET(m) was assumed to be AET(m) = PE(m)$S(m-1)/S_{max}$, in which PE(m) is monthly potential evaporation estimated with Penman–Monteith equation (mm) and S_{max} is parameter for the maximum storage (mm). Here, we assumed $S_{max} = 500$ and set the initial value of S as 400 (mm) at the beginning of year (i.e., we reset S on 1 January).

Figures A3 and A4 illustrate the monthly mean of calculated storages with raw dataset P_{raw} and P_{cor}, respectively. The monthly storage calculated with P_{raw} declined at the end of each year, especially in snow dominant catchments (Fig. A3), while the monthly storge calculated with P_{cor} recovered to the initial state (i.e., 400 mm) at the end of year (Fig. A4), suggesting that the correction of precipitation was successful in terms of the annual water balance.

HESSD
12, 9655–9700, 2015

Acknowledgements. The first author acknowledges funding support by NARO Grant for Research Abroard to conduct this study. The authors acknowledge Anne Jefferson and Dingbao Wang for providing the data for this study. The authors would also like to thank Luke Pangle and Antônio Meira, whose feedback on a draft manuscript greatly improved the final paper.

References

Anderson, R. S. and Anderson, S. P.: Geomorphology: The Mechanics and Chemistry of Landscapes, Cambridge University Press, 2010. 9669

Arnold, J. G. and Allen, P. M.: Automated methods for estimating baseflow and ground water recharge from streamflow records, J. Am. Water Resour. Assoc., 35, 411–424, 1999. 9663

Berghuijs, W. R., Sivapalan, M., Woods, R. A., and Savenije, H. H. G.: Patterns of similarity of seasonal water balances: a window into streamflow variability over a range of time scales, Water Resour. Res., 50, 5638–5661, doi:10.1002/2014WR015692, 2014. 9658

Blöschl, G., Sivapalan, M., and Wagener, T.: Runoff Prediction in Ungauged Basins: Synthesis Across Processes, Places and Scales, Cambridge University Press, 2013. 9657

Bouchet, R.: Evapotranspiration réelle et potentielle, signification climatique, IAHS-AISH P., 62, 134–142, 1963. 9662

Brutsaert, W. and Stricker, H.: An advection-aridity approach to estimate actual regional evapotranspiration, Water Resour. Res., 15, 443–450, 1979. 9662

Budyko, M.: Climate and life, Academic Press, New York, 508 pp., 1974. 9659, 9663

Carrillo, G., Troch, P. A., Sivapalan, M., Wagener, T., Harman, C., and Sawicz, K.: Catchment classification: hydrological analysis of catchment behavior through process-based modeling along a climate gradient, Hydrol. Earth Syst. Sci., 15, 3411–3430, doi:10.5194/hess-15-3411-2011, 2011. 9671

Eckhardt, K.: How to construct recursive digital filters for baseflow separation, Hydrol. Process., 19, 507–515, 2005. 9663

Gentine, P., D'Odorico, P., Lintner, B. R., Sivandran, G., and Salvucci, G.: Interdependence of climate, soil, and vegetation as constrained by the Budyko curve, Geophys. Res. Lett., 39, L19404, doi:10.1029/2012GL053492, 2012. 9659

Geographic Survey Institute, Japan: Geographic Data Download Service, available at: http://fgd.gsi.go.jp/download/, last access: 23 August 2015.

HESSD

12, 9655–9700, 2015

Geological Survey of Japan: Seamless Digital Geological Map of Japan 1 : 200 000, 2012 version, Research Information Database DB084, Geological Survey of Japan, Tsukuba, 2012.
Harman, C. and Troch, P. A.: What makes Darwinian hydrology "Darwinian"? Asking a different kind of question about landscapes, Hydrol. Earth Syst. Sci., 18, 417–433, doi:10.5194/hess-18-417-2014, 2014. 9657, 9671
Japan Meteorological Agency: Mesh Climatic Data of Japan, Tokyo, 2002.
Jefferson, A. J., Grant, G., Lewis, S., and Lancaster, S.: Coevolution of hydrology and topography on a basalt landscape in the Oregon Cascade Range, USA, Earth Surf. Proc. Land., 35, 803–816, 2010. 9658, 9667, 9668
Jefferson, A. J., Ferrier, K. L., Perron, J. T., and Ramalho, R.: Controls on the Hydrological and Topographic Evolution of Shield Volcanoes and Volcanic Ocean Islands, The Galapagos: A Natural Laboratory for the Earth Sciences, Geophys. Monogr. Ser., 204, 185–213, doi:10.1002/9781118852538, 2014. 9668
Kroll, C., Luz, J., Allen, B., and Vogel, R. M.: Developing a watershed characteristics database to improve low streamflow prediction, J. Hydrol. Eng., 9, 116–125, 2004. 9663
Lohse, K. A. and Dietrich, W. E.: Contrasting effects of soil development on hydrological properties and flow paths, Water Resour. Res., 41, W12419, doi:10.1029/2004WR003403, 2005. 9658, 9667, 9668
McDonnell, J., Sivapalan, M., Vaché, K., Dunn, S., Grant, G., Haggerty, R., Hinz, C., Hooper, R., Kirchner, J., Roderick, M. L., Selker, J., and Weiler, M.: Moving beyond heterogeneity and process complexity: a new vision for watershed hydrology, Water Resour. Res., 43, W07301, doi:10.1029/2006WR005467, 2007. 9657
Milly, P.: Climate, soil water storage, and the average annual, Water Resour. Res., 30, 2143–2156, 1994. 9659
Ministry of Land, Infrastructure and Transportation, Japan: National Land Numerical Information Download Service, available at: http://nlftp.mlit.go.jp/ksj-e/index.html, last access: 23 August 2015.
Morton, F. I.: Estimating evapotranspiration from potential evaporation: practicality of an iconoclastic approach, J. Hydrol., 38, 1–32, 1978. 9662
Murata, Y. and Kano, K.: The areas of the geologic units comprising the Japanese islands, calculated by using the Geological Map of Japan 1 : 1,000,000, 3rd Edn., CD-Rom version, Chishitsu News, 493, 26–29, 1995. 9660

HESSD
12, 9655–9700, 2015

Mushiake, K., Takahashi, Y., and Ando, Y.: Effects of basin geology on river flow regime in mountainous areas of Japan, Proc. Jpn. Soc. Civ. Eng., 1981, 51–62, 1981. 9658
National Institute for Land and Infrastructure Management, Japan: Japanese Dam Database, available at: http://dam5.nilim.go.jp/dam/, last access: 23 February 2015.
Ossaka, J., Ozawa, T., Nomara, T., Ossaka, T., Hirabayashi, J., Takaesu, A., and Hayashi, T.: Variation of chemical compositions in volcanic gases and water at Kusatsu-Shirane Volcano and its activity in 1976, B. Volcanol., 43, 207–216, 1980. 9670
Otsuki, K., Mitsuno, T., and Maruyama, T.: Comparison between water budget and complementary relationship estimates of catchment evapotranspiration – studies on the estimation of actual evapotranspiration (2), Transact. Japanese Soc. Irrig. Drai. Rural Eng., 112, 17–23, 1984. 9662
Sawicz, K., Wagener, T., Sivapalan, M., Troch, P. A., and Carrillo, G.: Catchment classification: empirical analysis of hydrologic similarity based on catchment function in the eastern USA, Hydrol. Earth Syst. Sci., 15, 2895–2911, doi:10.5194/hess-15-2895-2011, 2011. 9663
Sivapalan, M.: Process complexity at hillslope scale, process simplicity at the watershed scale: is there a connection?, Hydrol. Process., 17, 1037–1041, 2003. 9657
Sivapalan, M., Yaeger, M. A., Harman, C. J., Xu, X., and Troch, P. A.: Functional model of water balance variability at the catchment scale: 1. Evidence of hydrologic similarity and space-time symmetry, Water Resour. Res., 47, W02522, doi:10.1029/2010WR009568, 2011. 9658, 9659, 9671
Sivapalan, M., Savenije, H. H., and Blöschl, G.: Socio-hydrology: a new science of people and water, Hydrol. Process., 26, 1270–1276, 2012. 9657
Suzuki, T.: Rate of erosion in strato-volcanoes in Japan, Bull. Volcanol. Soc. Jpn., 14, 133–147, 1969. 9668
Taira, A.: Tectonic evolution of the Japanese island arc system, Annu. Rev. Earth Pl. Sc., 29, 109–134, 2001. 9660
Troch, P. A., Martinez, G. F., Pauwels, V., Durcik, M., Sivapalan, M., Harman, C., Brooks, P. D., Gupta, H., and Huxman, T.: Climate and vegetation water use efficiency at catchment scales, Hydrol. Process., 23, 2409–2414, 2009. 9659
Troch, P. A., Carrillo, G., Sivapalan, M., Wagener, T., and Sawicz, K.: Climate-vegetation-soil interactions and long-term hydrologic partitioning: signatures of catchment co-evolution, Hydrol. Earth Syst. Sci., 17, 2209–2217, doi:10.5194/hess-17-2209-2013, 2013. 9657, 9671

HESSD
12, 9655–9700, 2015

Troch, P. A., Lahmers, T., Meira, A., Mukherjee, R., Pedersen, J. W., Roy, T., and Valdés-Pineda, R.: Catchment coevolution: a useful framework for improving predictions of hydrological change?, Water Resour. Res., 51, 4903–4922, doi:10.1002/2015WR017032, 2015. 9657, 9659, 9667

Vogel, R. M. and Kroll, C. N.: Regional geohydrologic–geomorphic relationships for the estimation of low-flow statistics, Water Resour. Res., 28, 2451–2458, 1992. 9663

Wagener, T., Sivapalan, M., Troch, P., and Woods, R.: Catchment classification and hydrologic similarity, Geogr. Compass, 1, 901–931, doi:10.1111/j.1749-8198.2007.00039.x, 2007. 9657

Wagener, T., Blöschl, G., Goodrich, D., Gupta, H., Sivapalan, M., Tachikawa, Y., Troch, P., and Weiler, M.: A synthesis framework for runoff predictions in ungauged basins, in: chapt. 2, Runoff Predictions in Ungauged Basins, edited by: Blöschl, G., Sivapalan, M., Wagener, T., Viglione, A., and Savenije, H., Cambridge University Press, Cambridge, UK, 11–28, 2013. 9657

Wang, D. and Wu, L.: Similarity of climate control on base flow and perennial stream density in the Budyko framework, Hydrol. Earth Syst. Sci., 17, 315–324, doi:10.5194/hess-17-315-2013, 2013. 9659, 9666, 9668

Yadav, M., Wagener, T., and Gupta, H.: Regionalization of constraints on expected watershed response behavior for improved predictions in ungauged basins, Adv. Water Resour., 30, 1756–1774, 2007. 9664

Yokoyama, K., Ohno, H., Kominami, Y., Inoue, S., and Kawakata, T.: Performance of Japanese precipitation gauges in winter, J. Jpn. Soc. Snow Ice, 65, 303–316, 2003. 9673

Zhang, X., Zhang, L., Zhao, J., Rustomji, P., and Hairsine, P.: Responses of streamflow to changes in climate and land use/cover in the Loess Plateau, China, Water Resour. Res., 44, W00A07, doi:10.1029/2007WR006711, 2008. 9664

Zomer, R. J., Trabucco, A., Bossio, D. A., and Verchot, L. V.: Climate change mitigation: a spatial analysis of global land suitability for clean development mechanism afforestation and reforestation, Agr. Ecosyst. Environ., 126, 67–80, 2008. 9667

HESSD
12, 9655–9700, 2015

Table 1. List of study catchments.

Catchment Name	ID	Age (Ma)	Volcanic Coverage (–)	Area (km^2)
Shinaki	SNK	0.225	0.994	30.9
Tamagawa	TMG	2.78	0.852	287.0
Aseishigawa	ASE	3.52	0.940	225.5
Kawamata	KWM	3.69	0.507	179.4
Shimouke	SIM	4.00	0.982	185.0
Gosho	GOS	6.39	0.750	635.0
Naruko	NAR	8.43	0.598	210.0
Ikari	IKR	10.7	0.653	271.2
Aimata	AIM	11.7	0.603	110.8
Ishibuchi	ISB	11.8	0.732	154.0
Kamafusa	KAM	12.8	0.621	195.3
Shichikashuku	SCK	13.9	0.619	230.9
Yuda	YUD	18.5	0.633	583.0
Hazi	HAZ	82.2	0.623	217.0

HESSD
12, 9655–9700, 2015

Table 2. Estimated climate variables and indices.

ID	P_{cor} (mm yr^{-1})	PE (mm yr^{-1})	Q (mm yr^{-1})	E_{cor} (mm yr^{-1})	E_a (mm yr^{-1})	PE/P	E_{cor}/P
ASE	2215	903	1743	471	753	0.408	0.213
TMG	2937	916	2700	237	754	0.312	0.081
GOS	2544	976	1908	636	780	0.384	0.25
YUD	3206	955	2316	890	727	0.298	0.278
ISB	3305	928	2541	763	743	0.281	0.231
NAR	2852	941	2202	649	752	0.33	0.228
SCK	2100	1028	1326	774	807	0.49	0.369
KAM	2074	1024	1498	576	782	0.494	0.278
IKR	1770	1006	1301	469	792	0.568	0.265
KWM	2333	947	1404	928	783	0.406	0.398
AIM	2652	1026	1679	973	839	0.387	0.367
SNK	2454	932	1770	684	864	0.38	0.279
HAZ	1513	1249	573	939	895	0.826	0.621
SIM	3112	1229	2267	844	899	0.395	0.271

HESSD
12, 9655–9700, 2015

Table 3. Results of hydrometric and landscape analysis of study catchments.

ID	Age	PE/P	E/P	Drainage Density ($km\,km^{-2}$)	Baseflow index (Q_b/Q)	Baseflow coefficient (Q_b/P)	Slope of FDC
SNK	0.225	0.380	0.352	1.080	0.835	0.602	0.322
TMG	2.78	0.312	0.257	0.882	0.713	0.656	0.850
ASE	3.52	0.408	0.340	0.887	0.775	0.610	0.585
KWM	3.69	0.406	0.336	0.898	0.737	0.444	0.827
SIM	4.00	0.395	0.289	0.859	0.585	0.426	0.880
GOS	6.39	0.384	0.307	1.000	0.684	0.513	0.870
NAR	8.43	0.330	0.264	0.736	0.707	0.546	0.668
IKR	10.7	0.568	0.448	0.867	0.708	0.520	0.776
AIM	11.7	0.387	0.316	0.771	0.712	0.451	1.071
ISB	11.8	0.281	0.225	0.969	0.666	0.512	1.034
KAM	12.8	0.494	0.377	0.707	0.680	0.491	0.735
SCK	13.9	0.490	0.384	0.793	0.710	0.448	0.754
YUD	18.5	0.298	0.227	0.948	0.663	0.479	1.011
HAZ	82.2	0.826	0.592	0.777	0.533	0.202	0.895

HESSD
12, 9655–9700, 2015

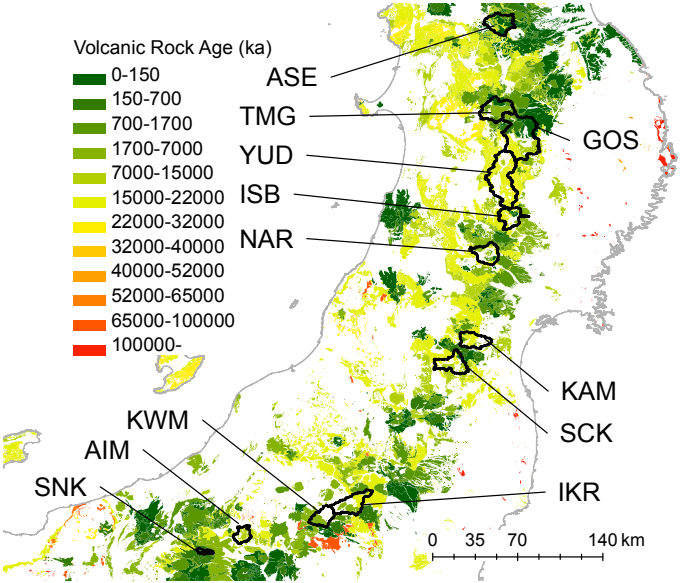

Figure 1. Study catchments in north-eastern Japan.

HESSD
12, 9655–9700, 2015

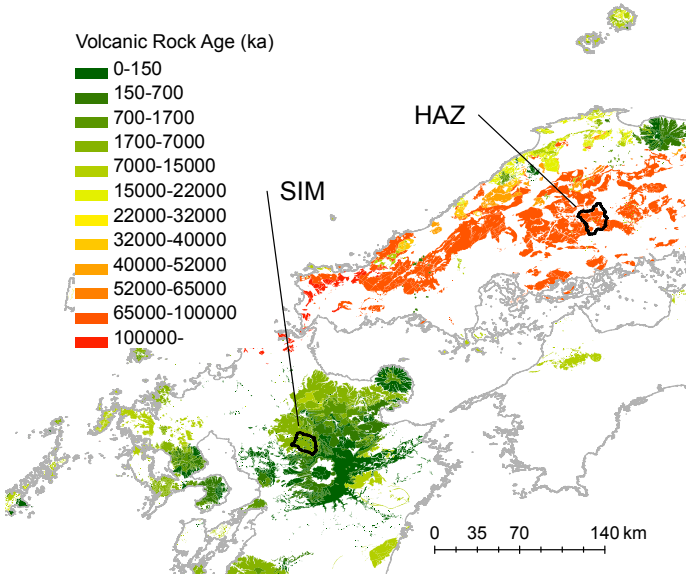

Figure 2. Study catchments in western Japan.

HESSD
12, 9655–9700, 2015

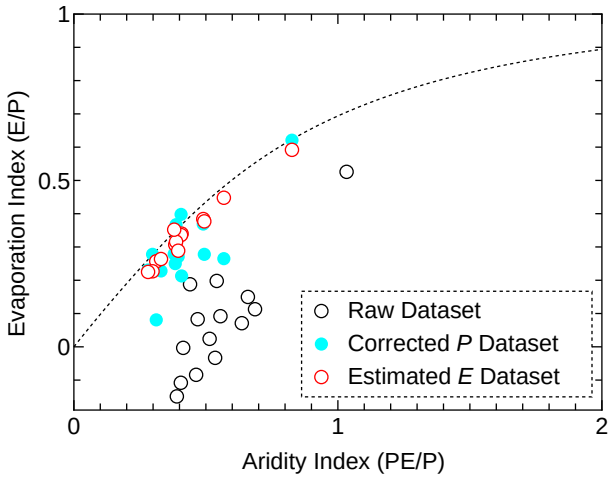

Figure 3. Raw, corrected P and estimated E datasets plotted with Budyko curve.

HESSD
12, 9655–9700, 2015

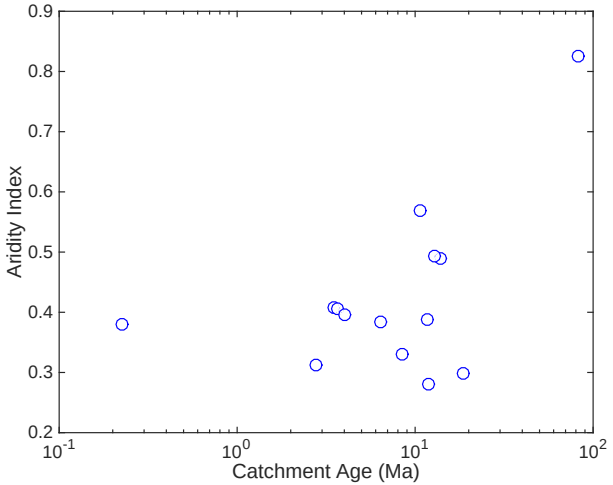

Figure 4. Relation between aridity index and age for the study catchments.

HESSD
12, 9655–9700, 2015

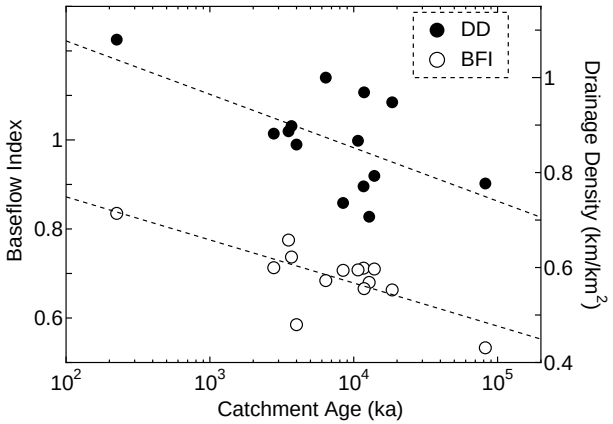

Figure 5. Influence of catchment age on baseflow index ($R = -0.756$, $p = 0.0017$) and drainage density ($R = -0.603$, $p = 0.0222$).

HESSD
12, 9655–9700, 2015

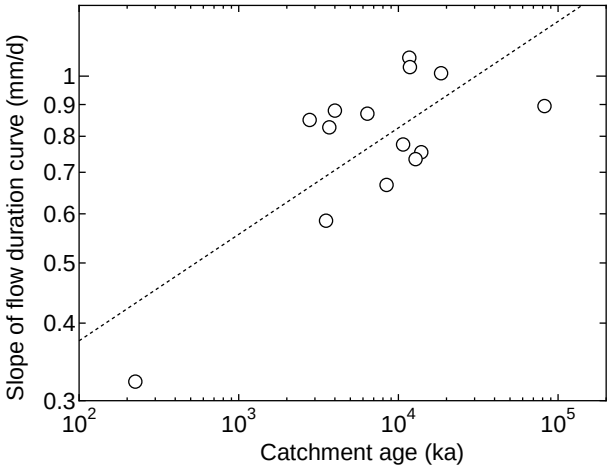

Figure 6. Slope of flow duration curves with catchment age (R = 0.74, p = 0.002).

HESSD
12, 9655–9700, 2015

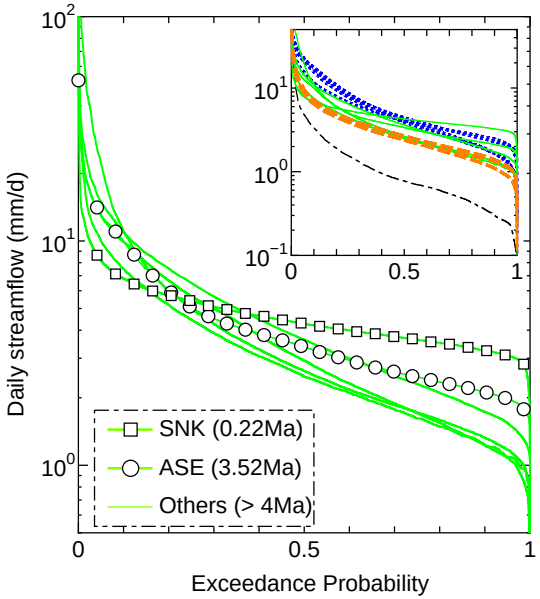

Figure 7. Flow duration curves for the catchments whose aridity index are in the range between 0.35 and 0.45. Inset of this figure illustrates flow duration curves for all study catchments. Each colored line represents data from a certain range in aridity index (key to line colors is as follows: blue: $PE/P < 0.35$; green: $0.35 < PE/P < 0.45$; orange: $0.45 < PE/P < 0.65$ and black: $PE/P > 0.65$).

HESSD
12, 9655–9700, 2015

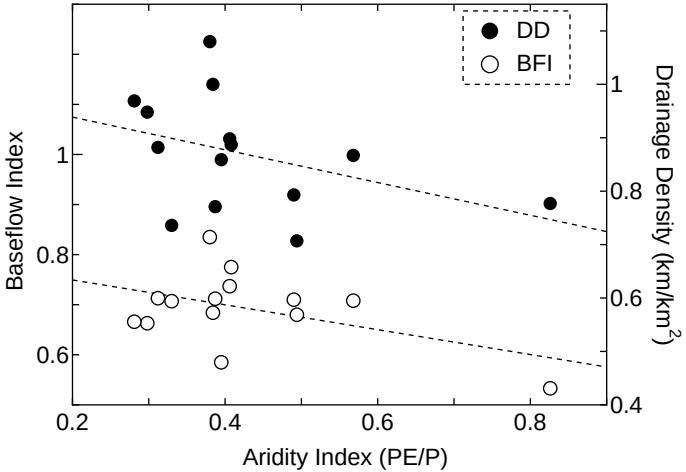

Figure 8. Climate controls on baseflow index and drainage density. The relationships with aridity index were weak for both drainage density ($R = -0.451$, $p = 0.105$) and baseflow index ($R = -0.372$, $p = 0.190$).

HESSD
12, 9655–9700, 2015

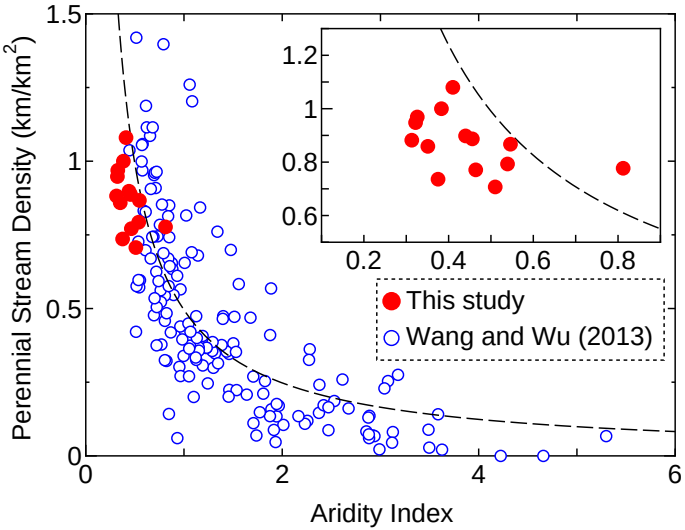

Figure 9. Perennial stream density (D_p) and aridity index (PE/P). The dashed line represents the fitted curve (D_p = 0.444/(PE/P)) from Wang and Wu (2013).

HESSD
12, 9655–9700, 2015

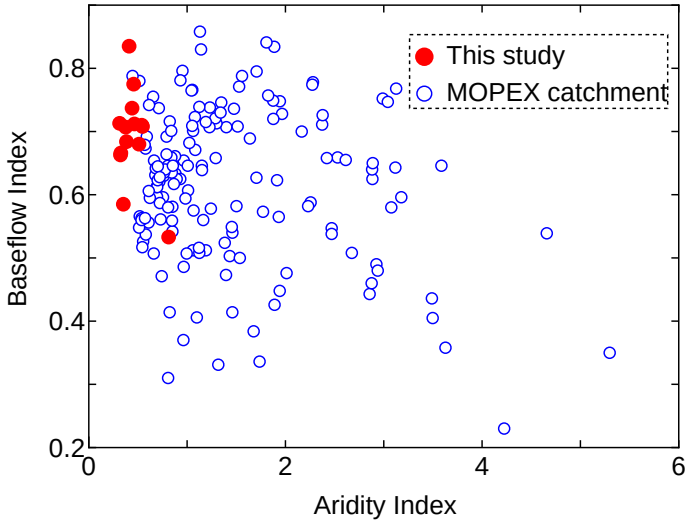

Figure 10. Relation between baseflow index and aridity index in Japan and MOPEX catchments in the US. Aridity index does not explain variability in baseflow index.

HESSD
12, 9655–9700, 2015




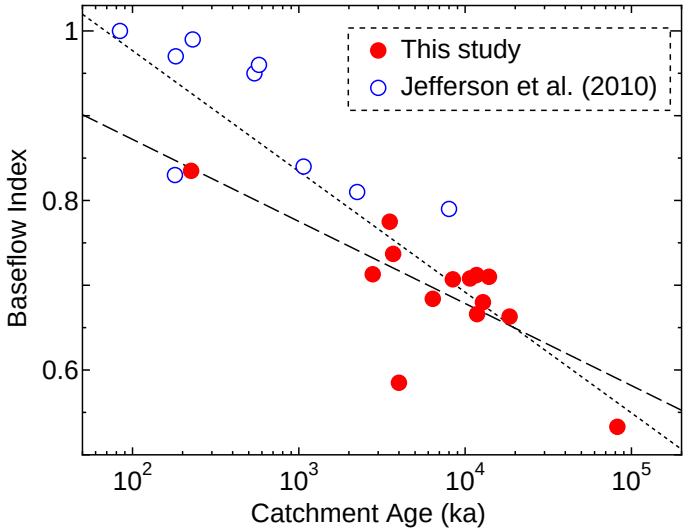

Figure 11. Baseflow index with catchment age. Dashed line is regressed line for the study catchments ($R = -0.756$, $p = 0.0017$). Dotted line is regressed line for the integrated dataset of the catchments in Japan and the Oregon Cascades from Jefferson et al. (2010) ($R = -0.879$, $p < 0.001$).

HESSD
12, 9655–9700, 2015

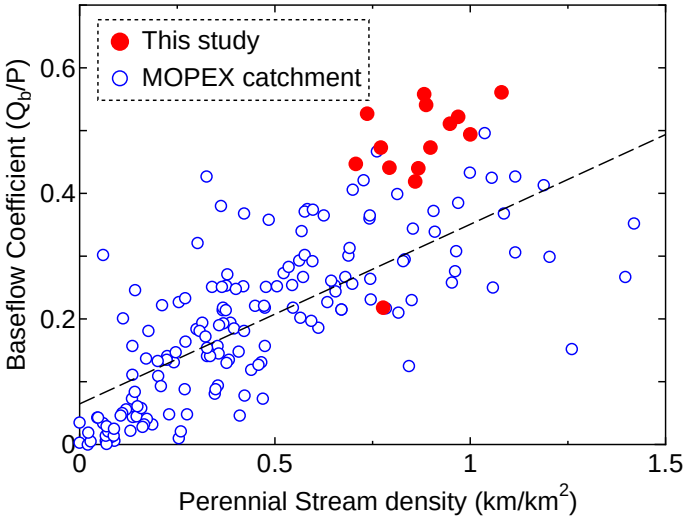

Figure 12. Perennial stream density and baseflow coefficient (Q_b/P). The baseflow, Q_b, in their study was estimated by using the same equation and parameter value as we used in Eq. (3). The correlation efficient between them was 0.74 without the study catchments (Wang and Wu, 2013).

HESSD
12, 9655–9700, 2015

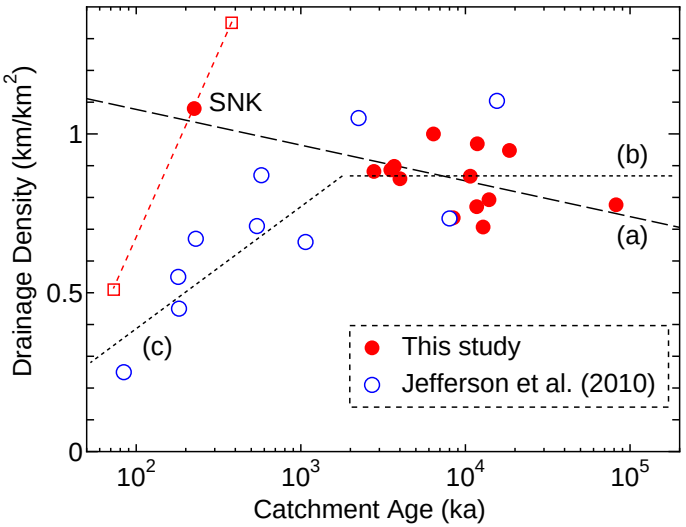

Figure 13. Drainage density with catchment age. Line (a) is the regression line for the study catchments ($R = -0.603$, $p = 0.0222$). Line (b) is the mean drainage density for the catchments older than 2 Ma in Japan and the Oregon Cascades (0.873 km km^{-2}). Line (c) is the regressed line for younger than 2 Ma in the Oregon Cascades. The drainage densities and basalt ages of the upper and lower part of SNK are plotted as squares (the upper part: drainage density is 0.51 km km^{-2} and basalt age is 72 kyr; the lower part: 1.35 km km^{-2} and 380 kyr).

HESSD
12, 9655–9700, 2015

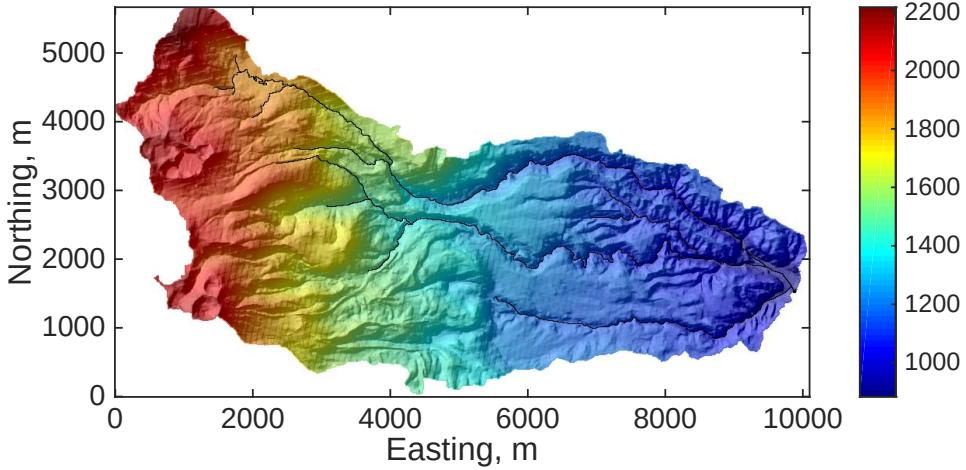

Figure 14. Topography and stream networks in SNK catchment.

HESSD
12, 9655–9700, 2015

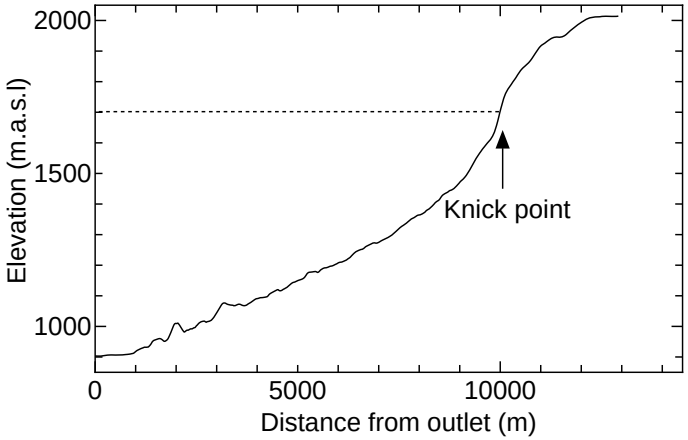

Figure 15. Longitudinal profile of the longest stream in SNK. Knick point is identified as the point at which the stream slope is the steepest.

HESSD
12, 9655–9700, 2015

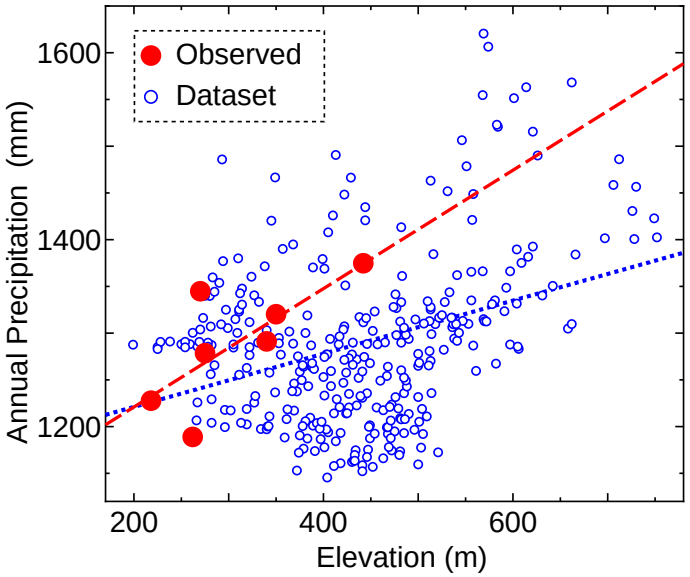

Figure A1. Altitudal distribution of precipitation (HAZ catchment, annual).

HESSD
12, 9655–9700, 2015

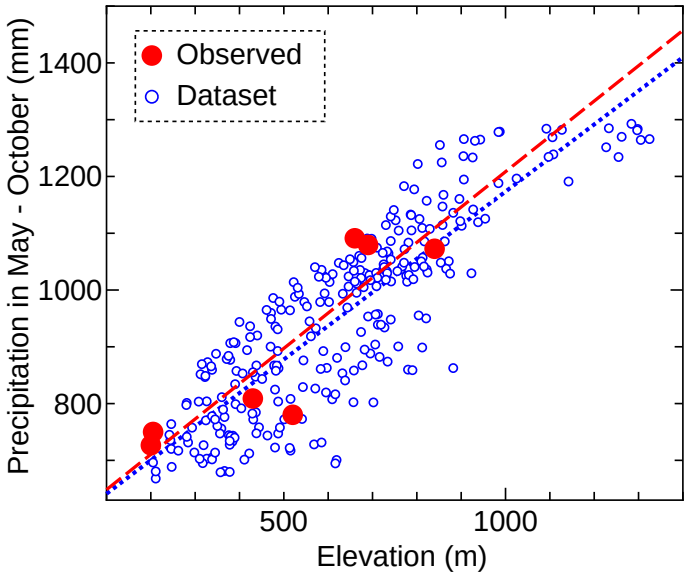

Figure A2. Altitudal distribution of precipitation with elevation (ASE catchment, May–October).

HESSD
12, 9655–9700, 2015

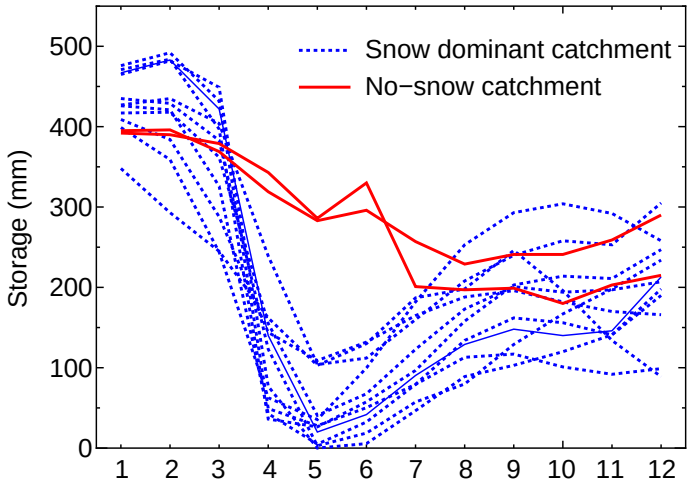

Figure A3. Seasonal water balance for raw dataset.

HESSD
12, 9655–9700, 2015

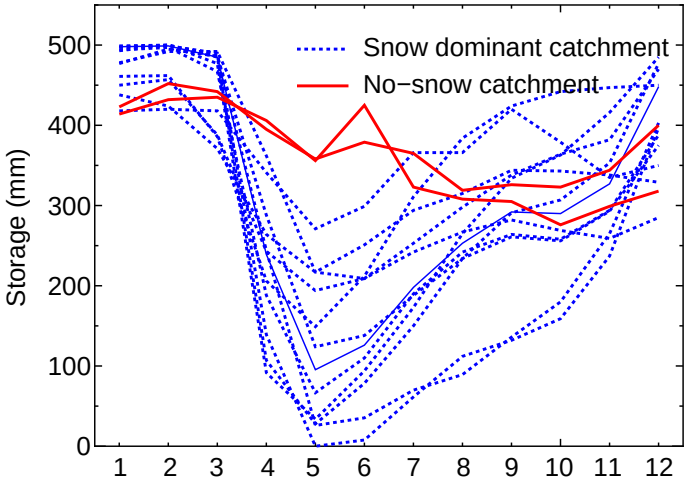

Figure A4. Seasonal water balance for precipitation corrected dataset.

HESSD
12, 9655–9700, 2015